PNAS RESEARCH ARTICLE | EARTH, ATMOSPHERIC, AND PLANETARY SCIENCES OPEN ACCESS

Metastable state preceding shear zone instability: Implications for earthquake-accelerated landslides and dynamic triggering

Yan Li[a], Wei Hu[a,1], Qiang Xu[a], Hui Luo[a], Chingshung Chang[b], and Xiaoping Jia[c]

Affiliations are included on p. 9.

Edited by David Weitz, Harvard University, Cambridge, MA; received September 4, 2024; accepted November 24, 2024

Understanding the dynamic response of granular shear zones under cyclic loading is fundamental to elucidating the mechanisms triggering earthquake-induced landslides, with implications for broader fields such as seismology and granular physics. Existing prediction methods struggle to accurately predict many experimental and in situ landslide observations due to inadequate consideration of the underlying physical mechanisms. The mechanisms that influence landslide dynamic triggering, a transition from static (or extremely slow creeping) to rapid runout, remain elusive. Herein, we focus on the inherent physics of granular shear zones under dynamic loading using ring shear experiments. Except for coseismic slip caused by the dynamic load, varying magnitudes of postseismic creep with increasing cycles of dynamic loading are observed, highlighting the effects of coseismic weakening (shear zone fatigue) and subsequent postseismic healing. A metastable state, characterized by a significant increase in postseismic creep, typically precedes shear zone instability. The metastable state may arise as weakened shear resistance approaches the applied shear stress, demonstrating a phase transition from a solid-like state to a fluid state (plastic granular flow). The metastable state may potentially indicate the shear zone's stress state and serve as a precursor to impending instability. Furthermore, the proposed mechanisms offer a compelling explanation for the widespread postseismic landslide movement following earthquakes. Incorporating these mechanisms into the Newmark method has the potential to improve the prediction of earthquake-induced landslide displacement and enhance our understanding of dynamic triggering.

earthquake-induced landslides | dynamic triggering | co-seismic weakening | healing effect | granular material

Significance

Earthquake-triggered landslides can cause catastrophic disasters, yet existing prediction methods struggle to accurately predict their motion and failure due to inadequate consideration of the underlying physical mechanisms. We conducted experiments to simulate its dynamic triggering, from static to rapid runout, and reveal that coseismic weakening and postseismic healing substantially influence the processes. We observed that postseismic creep, in addition to the expected coseismic slip, is highly sensitive to the shear zone state. A metastable state, characterized by significantly increased postseismic creep, typically precedes shear zone instability, underlying a phase transition from solid-like behavior to plastic flow. By incorporating coseismic weakening and postseismic healing, a modified method is proposed to potentially improve the prediction of landslide dynamic responses to seismic events.

Earthquakes are a primary trigger of landslides in mountainous regions, often causing widespread devastation and resulting in long-term geohazards (1–3). For instance, the 1999 Chi-Chi earthquake in Taiwan triggered over 20,000 landslides (4). The 2008 Wenchuan earthquake in China resulted in over 60,000 landslides and extensive subsequent geohazards (3). Understanding the seismic response of landslide shear zones, the most critical geological structure governing slope stability, is essential for unraveling the mechanisms of landslide dynamic triggering (4, 5). Moreover, further investigation is still needed to fully explain observed earthquake-induced phenomena, such as earthquake-accelerated landslides and delayed-trigger landslides (6–10). The relevant research has potential implications not only for landslides but also for other geological processes, including fault weakening and earthquake triggering (11–15), and even for granular physics (16–18).

Previous studies have explored various mechanisms for earthquake-induced landslides. A simplified approach (Newmark method) models landslides as blocks on slopes, with shear zone friction governed by the Mohr–Coulomb law (1, 2, 7, 19). However, this simplified model fails to capture the varying of shear zone strength during seismic events. Another prominent hypothesis, seismic liquefaction, attributes earthquake-induced landslides to the weakening of water-saturated shear zones. This weakening is thought to result from the buildup of excess pore water pressure, which reduces the effective shear resistance of the shear zone (20). The grain-crushing-induced contraction is also thought to contribute to excess pore pressure and facilitate liquefaction (21, 22). In addition, particle fragmentation and the resulting grain size reduction are believed to weaken shear zones (2, 9). While these hypotheses acknowledge the complex geological factors at play, such as pore water pressure and particle fragmentation, a fundamental question remains—will seismic loading inherently affect the strength of a pure granular shear zone.

Some pioneer researchers have demonstrated that seismic waves can weaken the shear resistance of idealized granular materials, even in the absence of pore fluid pressure or grain crushing (11, 16, 23). However, the employed dynamic loading conditions do not accurately

Author contributions: Y.L. and W.H. designed research; Y.L., W.H., and H.L. performed research; Y.L. and W.H. contributed new reagents/analytic tools; Y.L., W.H., Q.X., C.C., and X.J. analyzed data; and Y.L. and W.H. wrote the paper.

The authors declare no competing interest.

This article is a PNAS Direct Submission.

[1]To whom correspondence may be addressed. Email: huwei1999@126.com.

This article contains supporting information online at https://www.pnas.org/lookup/suppl/doi:10.1073/pnas.2417840121/-/DCSupplemental.

Published December 30, 2024.

represent the mechanical setting that typically triggers landslides. For instance, the experiments may be conducted with a constant strain rate (24–27) or extremely high peak velocity in each dynamic cycle (4, 28). The mechanical process may not accurately represent landslide triggering, which involves a transition from a static state (or extremely slow creeping) to a rapid runout. In addition, the high confining pressures (e.g., 20 MPa) often used in fault simulation experiments, where mechanisms like thermal pressurization and vaporization are observed (29–31), limit their applicability to landslide shear zones, which typically experience much lower confining pressures (generally less than a few MPa). Critically, strain-controlled experiments focus on characterizing friction variations at specific shear velocities. Through the strain-controlled approach, the transition phase from shear zone stable to instable, i.e., the metastable state, cannot be observed. This transition is essential for understanding the inherent physics of dynamic triggering mechanisms. Thus, force-controlled experiments, designed to simulate the almost constant driving force characteristic of landslides, are necessary to gain insight into these mechanisms.

To address these limitations, this study investigates the response of granular shear zones to dynamic loading through force-controlled ring shear experiments, replicating the stress and seismic frequency conditions analogous to real landslides. By progressively increasing the number of dynamic cycles until failure, we seek insight into the underlying mechanisms governing shear zone behavior. In addition to the expected coseismic slip, varying magnitudes of postseismic creep are observed, suggesting a potential weakening of shear resistance during the coseismic phase (an analog to fatigue) and a subsequent healing effect during the postseismic phase. By considering these mechanisms, we can better predict shear zone deformation and stability and shed light on the mechanisms driving earthquake-accelerated landslides and dynamic triggering.

Results

Earthquakes generate seismic waves that induce inertial force fluctuations of the slope mass, which can lead to dynamic landslide triggering. Shear zones are the most critical geological structures that determine landslide stability and are generally composed of granular material. Dynamic ring shear experiments were conducted under a similar mechanical condition derived from the characteristics of earthquake-induced landslides (Fig. 1). The pressure from the overburden is simulated by the applied normal stress, and the driven force is simulated by the shear stress. The seismic wave caused by the earthquake can be simulated by the cyclic loading applied. Real seismic waves are complex, involving various frequencies and acting in both normal and shear directions. We systematically apply increasing numbers of simple harmonic waves, starting from one cycle and continuing until shear zone instability, to understand the most inherent physics influencing the dynamic granular shear zone behavior.

Fig. 2 shows representative experimental results, conducted with a constant normal stress of 300 kPa (approximating the pressure within a moderate-scale landslide) and a dynamic shear stress of 194 kPa (25 kPa amplitude, 1 Hz frequency). Complete datasets for experiments with 1 to 14 dynamic cycles are provided in Supporting Information. Three distinct scenarios can be observed under varying numbers of dynamic cycles, and typical examples are shown in Fig. 2, under 8, 13, and 14 dynamic cycles, respectively.

Coseismic Slip and Postseismic Creep. Fig. 2*A* illustrates the response observed with a relatively low number of dynamic cycles. Each cycle generates a discrete step in shear deformation, characterized by acceleration and a subsequent step-like displacement when the applied dynamic shear stress surpasses the material's shear resistance. This characteristic displacement, induced by the peak dynamic shear stress in each cycle, is termed "coseismic slip."

Within each dynamic cycle, the applied sinusoidal wave comprises a crest phase (shear stress exceeding the mean value) and a trough phase (shear stress below the mean value). During the crest phase, when the peak dynamic shear stress surpasses the shear resistance, shear deformation occurs. Conversely, during the trough phase, shear deformation decelerates and ceases as the dynamic shear stress falls below the shear resistance. Fig. 2*A* illustrates this pattern, with shear velocity returning to zero during each trough phase. Notably, in the postseismic phase, where dynamic loading stops, almost no postseismic deformation is observed, consistent with predictions from the classical Newmark method (19).

Fig. 2 *B* and *C* illustrate the dynamic response under a higher number of dynamic cycles. Not only is there a step-like coseismic slip, an obvious shear deformation is observed during the postseismic phase. In Fig. 2*B*, postseismic creep reaches 0.7 mm within tens of seconds, on same order of magnitude of the coseismic slip. Fig. 2*C* shows the condition with higher number of dynamic

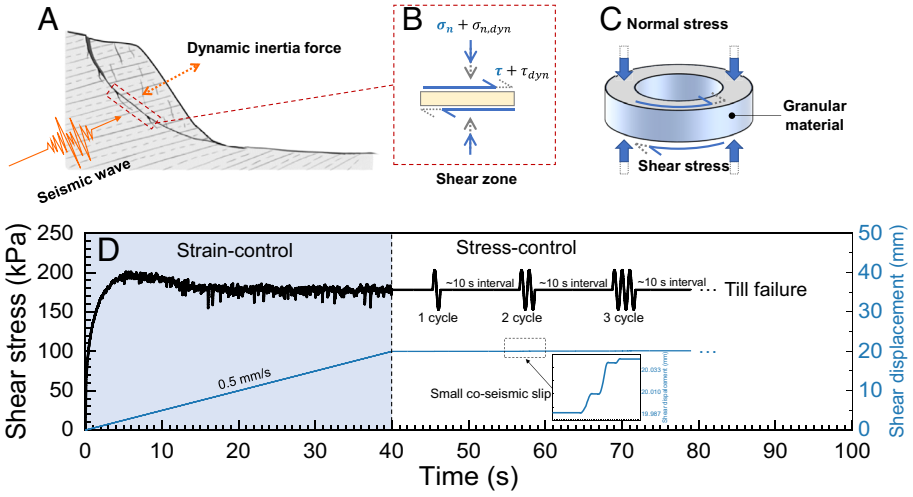

Fig. 1. Conceptual diagram for investigating the dynamic behavior of granular shear zones and the experimental sequence. (*A*) Schematic representation of a landslide influenced by seismic wave propagation. (*B*) Dynamic force fluctuations experienced by landslide shear zones due to seismic activity. (*C*) Simulation of long-distance shear using a ring-shear apparatus. (*D*) Experimental procedure involving an initial strain-controlled phase to reach a steady state, followed by a stress-controlled phase with progressively increasing dynamic cycles.

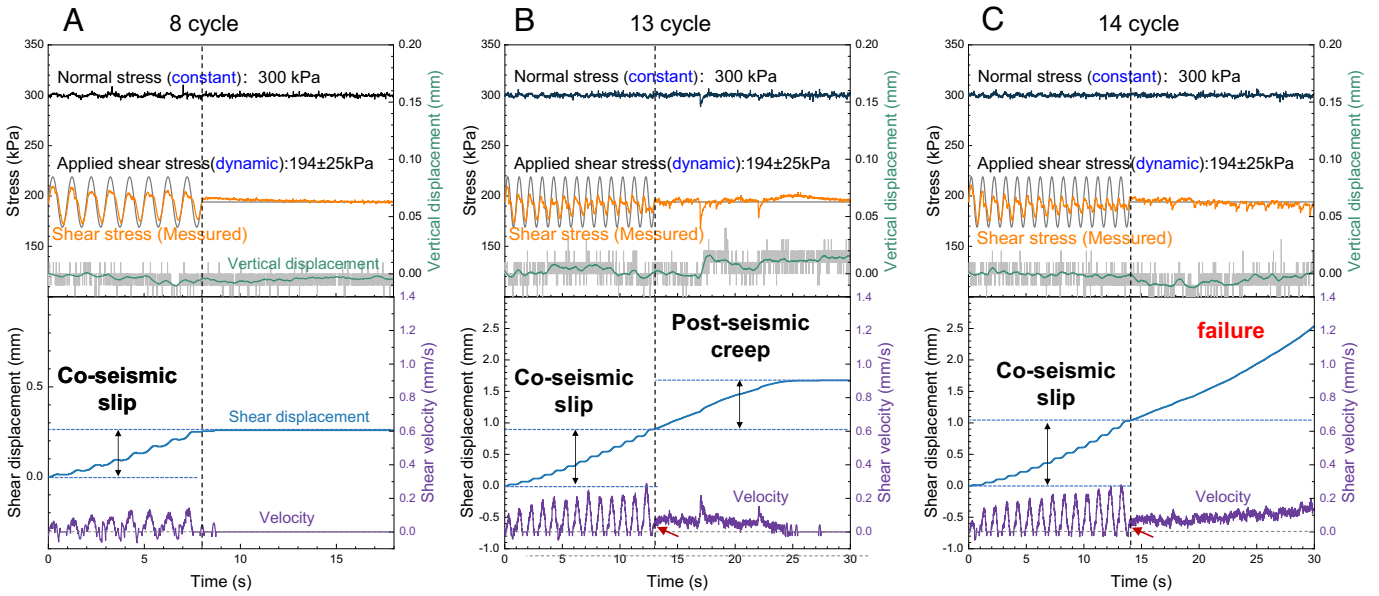

Fig. 2. Three distinct responses of granular shear zones to cyclic shear loading. (*A*) Negligible postseismic deformation under a low number of cycles, (*B*) significant postseismic creep emerging under a moderate number of cycles, and (*C*) shear zone failure occurring when the number of cycles exceeds a critical threshold.

cycles, the shear zone experienced continuous acceleration during the postseismic phase, ultimately resulting in shear zone failure. Although cessation of the seismic load should theoretically result in a stable shear zone, postseismic deformation is observed. These observations deviate from classical prediction models, such as the Newmark method, highlighting its limitations in fully capturing the complex dynamics of shear zone behavior under cyclic loading.

Analyzing the variation of shear velocity provides further insights into the dynamic processes. In cases under fewer dynamic cycles without postseismic creep (Fig. 2*A*), the shear velocity returns to zero during the last trough of the coseismic phase. In contrast, when significant postseismic slip occurs (Fig. 2 *B* and *C*), a positive shear velocity occurs at the end of the final trough phase (marked by red arrows in Fig. 2 *B* and *C*). This key observation indicates that the shear resistance is reduced below the mean dynamic shear stress during the last dynamic cycle, generating continued deformation even after the dynamic loading ceases.

Fig. 3 presents results from the experiment conducted with a lower applied shear stress of 182 kPa, while maintaining other experimental conditions (normal stress, amplitude, and frequency of dynamic loading) identical to those in Fig. 2. Under the lower applied shear stress, 182 kPa, the dynamic response of the granular shear zone differs significantly. Negligible postseismic creep is observed with increasing dynamic cycles, even after 40 dynamic cycles. However, the nonlinear increase in coseismic slip with increasing cycle number indicates that the shear resistance of the material is still progressively weakened during the dynamic phase.

Increasing Postseismic Creep Precedes Shear Zone Instability. Fig. 4 presents a statistical analysis of coseismic slip and postseismic creep for experimental series S05 (shear stress: 182 ± 25 kPa) and

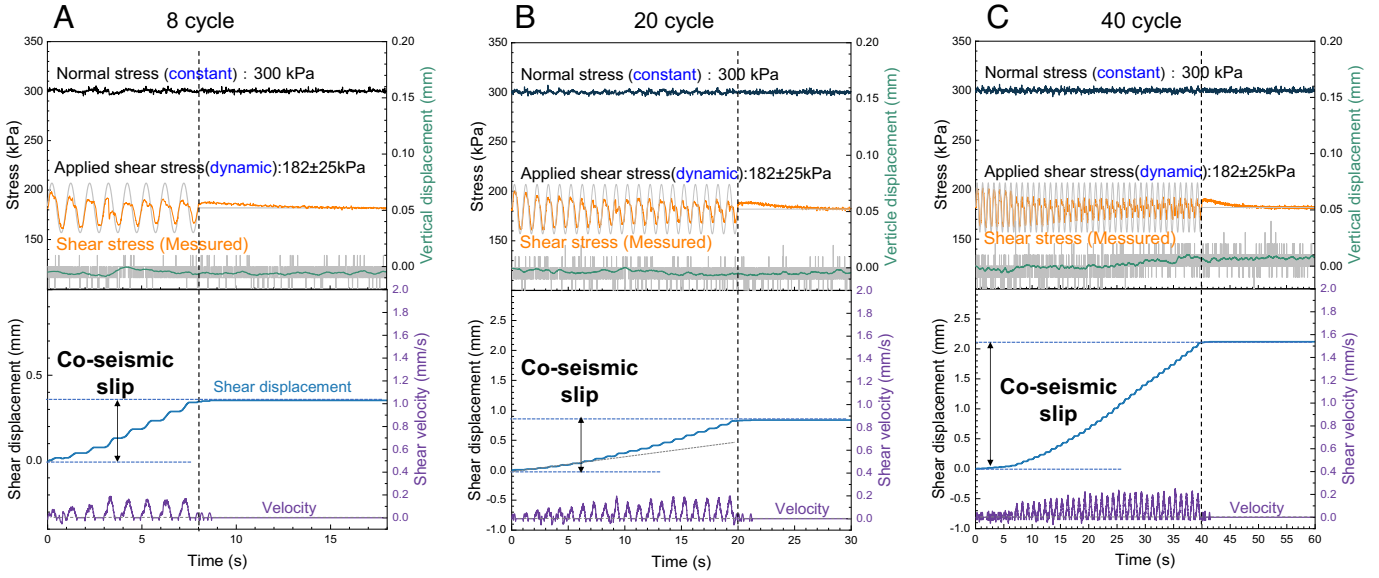

Fig. 3. Granular shear zone exhibits stable behavior under lower dynamic shear stress (182 ± 25 kPa) with (*A*) 8 cycles, (*B*) 20 cycles and (*C*) 40 cycles. The postseismic creep is negligible and the shear zone is stable even under 40 dynamic cycles.

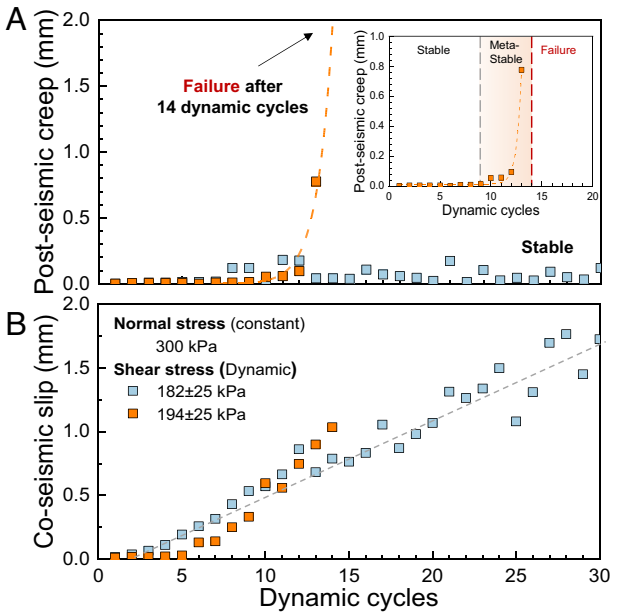

Fig. 4. Evolution of (*A*) postseismic creep and (*B*) coseismic slip with increasing dynamic cycles under varying shear stress levels. Experiments leading to shear zone failure exhibit a significant increase in postseismic creep prior to failure, while those remaining stable show negligible postseismic creep. These distinct trends highlight the potential of postseismic creep as a precursor to dynamic instability in granular shear zones.

S09 (shear stress: 194 ± 25 kPa). Under lower dynamic shear stress, the shear zone remains stable beyond 40 cycles, with postseismic creep remaining negligible regardless of the number of cycles. In contrast, under a higher shear stress, a significant increase in postseismic creep preceding shear zone instability can be observed.

Similar trends are observed when the dynamic load is in the normal stress direction, as shown in *SI Appendix*, Fig. S1. Under a limited number of dynamic cycles, postseismic creep remains negligible. However, as the number of cycles increases, postseismic creep becomes evident and continuously increases with dynamic cycles till shear zone instability (*SI Appendix*, Fig. S2). This pattern of increasing postseismic creep preceding failure, observed under both dynamic shear and normal stress conditions, suggests that dynamic loading from both the normal and shear direction can weaken the strength of the granular shear zone.

Fig. 5 and *SI Appendix*, Fig. S3 demonstrate the evolution of postseismic creep with increasing dynamic cycles under varying dynamic loads. A clear statistical trend emerges: postseismic creep significantly increases prior to shear zone instability. Higher applied mean shear stress corresponds to fewer cycles required to induce failure. In addition, in cases with substantially lower shear stress, shear zone failure is not observed, nor is a monotonic increase in postseismic creep. The underlying mechanisms will be further discussed in the following section.

Discussion

Our experimental observations demonstrate that shear zone resistance is not constant when subjected to dynamic loading. A coseismic-weakening effect significantly influences the response of granular shear zones to seismic loading. Meanwhile, a mere decrease of shear resistance cannot lead to the spontaneous stop of postseismic creep, as shown in Fig. 2*B*. As demonstrated in Fig. 6, we speculate that an interplay of coseismic weakening and postseismic healing effect causes the three distinct shear deformation patterns. In this section, we will further discuss the potential mechanisms underlying these effects and their implications.

Coseismic Weakening Effect. Seismic waves can weaken the strength of granular shear zones, as demonstrated by numerous studies (4, 11, 16, 23, 32). This seismic-induced weakening has been experimentally validated through observations of reduced shear modulus and quantitative analyses using both strain-rate-controlled (11, 23, 25, 32, 33) and velocity-controlled experiments (4). For instance, Togo et al. utilized a high shear velocity (0.65 m/s maximum velocity) to explain shear weakening and high-velocity weakening, employing the stress–strain curve obtained from high-speed experiments as a proxy for dynamic shear zone weakening (4). Similarly, strain-controlled experiments typically apply a constant shear velocity to measure variations in shear stress or shear modulus during vibration input. However, landslide dynamic triggering is a transition from a static (or extremely slow creeping) state to catastrophic rapid runout under an almost constant sliding force condition. With the strain-controlled approach, the metastable state, or more exactly, the transition from jamming to unjamming of granular shear zone, cannot be observed. This study adopts a stress-controlled approach, allowing more realistic mechanical settings to allow insights into the landslide dynamic triggering processes. Three phenomena observed in our experiments support the hypothesis of coseismic shear weakening:

a) Nonlinear increase in coseismic slip: Coseismic slip exhibits a nonlinear increase with successive dynamic cycles. Under conditions of constant shear resistance and simple harmonic loading, shear deformation should remain constant for each cycle. However, Figs. 2 and 3 illustrate that shear deformation during each dynamic step increases nonlinearly in the coseismic phase, indicating a gradual weakening of shear resistance.

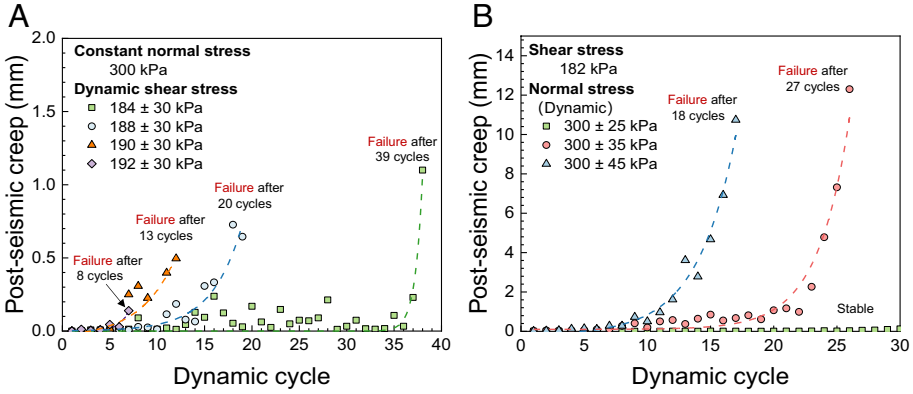

Fig. 5. Statistic of the coseismic slip evolution in the dynamic experiments. The coseismic slip will significantly increase proceeding to shear zone failure both under (*A*) dynamic shear stress and (*B*) dynamic normal stress conditions.

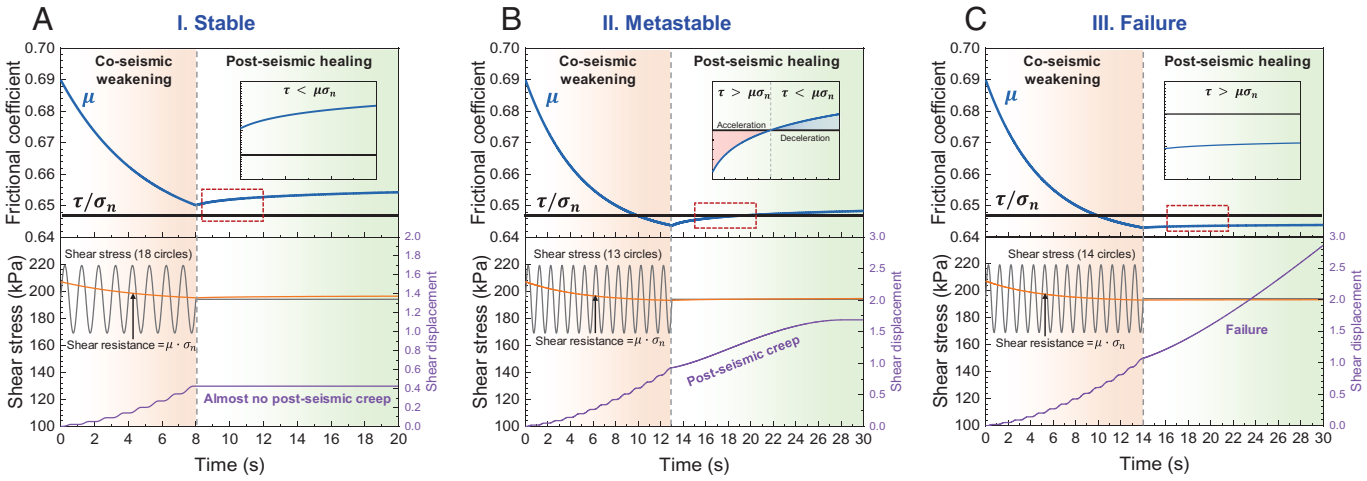

Fig. 6. Interplay of applied shear stress, dynamic shear resistance evolution (coseismic weakening and postseismic healing), and resultant shear displacement. Three scenarios are depicted: (*A*) Negligible postseismic deformation occurs when shear resistance remains above the applied shear stress. (*B*) Postseismic creep occurs when shear resistance weakens slightly below the applied shear stress, however, ultimately stabilizing when the shear resistance surpasses the applied stress due to the healing effect. (*C*) Catastrophic failure occurs when shear resistance weakens significantly below the applied shear stress and healing effect is suppressed due to the high strain rate.

b) Emergence of postseismic creep: Postseismic creep remains negligible under limited cycling, while it becomes increasingly apparent with successive dynamic cycles. This suggests that seismic waves can weaken shear resistance and even make it below the applied constant shear stress.

c) Shear wave decay: We observe a decay in shear wave propagation through the granular material during the dynamic loading phase (Fig. 2, highlighted in Fig. 7). While the applied dynamic shear stress at the sample base (see *Inset* of Fig. 7*A*) maintains a constant amplitude in each cycle, the measured shear stress amplitude at the sample top progressively decays. This decay suggests a gradual softening of the granular material during cyclic loading, as a proxy of the gradual decrease of shear resistance and shear modulus (11, 16), further supporting the hypothesis of dynamic shear resistance weakening.

The observed softening of the granular shear zone suggests a potential phase transition induced by dynamic loading. Initially, the measured shear stress matches the applied shear stress, indicating a quasistatic state within the granular shear zone. However, as the cyclic loading progresses, the measured shear stress amplitude gradually decreases under constant applied load, underlying a dynamic transition from solid-like to fluid-like behavior. This phenomenon aligns with the understanding that shear waves can hardly propagate through ideal fluids. Consequently, during this solid–fluid phase transition, the shear resistance and shear modulus progressively decay. Ultimately, the shear zone is unjammed and undergoes continuous plastic shear deformation. As this study focuses on the dynamic behavior of the shear zone, this solid-to-fluid transition represents the failure of the shear zone, not necessarily the complete fluidization of the entire landslide mass.

The observed weakening of shear resistance may arise from physics across multiple scales. At the microscopic level, seismic input can weaken asperity contacts, leading to a nonlinear reduction in granular material modulus (11, 16–18). Such microscopic contact weakening can subsequently influence the force network distribution within the granular system and may impact the behavior of the granular assembly at a macroscopic scale (32).

However, the observed shear deformation in this study (on the order of millimeters) significantly exceeds the particle size (approximately 0.2 mm). This discrepancy suggests that the dynamic shear resistance weakening cannot be solely attributed to microscopic asperity-scale processes but must also involve mechanisms operating at a larger scale. The observed phase transition, evidenced by the decay of shear wave propagation (Fig. 7), further supports the presence of macroscopic weakening mechanisms. Sufficient seismic wave input, equivalent to an increase of effective temperature, can substantially reduce the jamming limit of granular materials (34–36), inducing a transition from a solid-like to a fluid-like phase (14).

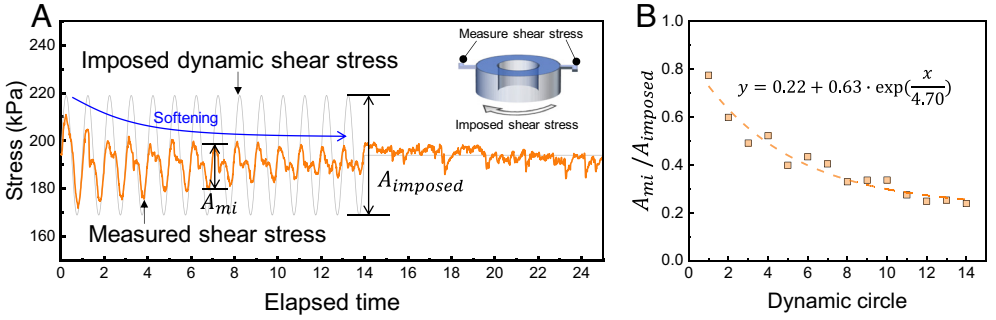

Fig. 7. A substantial decay of shear wave propagation during the dynamic phase. (*A*) A discrepancy between the applied dynamic shear stress at the bottom of the sample and the measured shear stress at its top, (*B*) and the ratio of the imposed and the measured shear stress at the two sides of the sample. This attenuation of shear stress response through the sample highlights a progressive "softening" phenomenon induced by the continuous dynamic loading.

While the mechanisms governing the dynamic weakening of shear strength are multiscale and undoubtedly complex, our experimental results clearly demonstrate their impact on the mechanical behavior of granular materials. In this work, we define coseismic weakening as follows:

Coseismic weakening: The reduction in shear resistance of the granular shear zone that occurs during vibration.

The vibration-induced weakening of shear resistance appears to approach a minimum limit, representing a steady state under sustained dynamic loading. This limit likely depends on the intensity and frequency of the seismic waves. We can express this shear resistance weakening process as an exponential function of dynamic cycles:

$$\mu(N) = \mu_0 + A \cdot \exp(-N/N_0), \quad [1]$$

where N is the dynamic cycle, μ_0 is the minimum shear resistance caused by vibration, N_0 determines the number of dynamic loads required for significant weakening, and A represents the weakening rate.

Further experiments reveal that both dynamic amplitude and frequency influence the weakening function described by Eq. **1**. Increasing dynamic amplitude (*SI Appendix*, Figs. S4–S8 and Table S2) or decreasing frequency (*SI Appendix*, Figs. S9–S12 and Table S3) results in the metastable state or shear zone failure with fewer dynamic cycles. These results indicate that the coseismic weakening effect becomes stronger with increasing amplitude or decreasing frequency. Furthermore, at extremely high dynamic amplitudes and low frequencies, shear resistance can drastically weaken compared to the driving force, leading to catastrophic landslide failure. In this condition, the shear zone may directly surpass its metastable state and transfer into catastrophic failure. However, the influence of dynamic frequency is complex and requires further investigation. It is important to acknowledge that changing frequency while maintaining a constant number of dynamic cycles also alters the duration of dynamic loading and the associated acceleration proportionally. Future research is needed to systematically investigate the individual and coupled effects of dynamic cycles, amplitude, and frequency on the coseismic weakening effect.

Postseismic Healing Effect. Seismic-induced weakening alone can explain the observed nonlinear coseismic slip and eventual shear zone failure (Fig. 2 *A* and *C*). However, it fails to fully account for the postseismic creep phenomenon observed in Fig. 2*B*. In this instance, the shear zone exhibits creep behavior under constant normal and shear stress, eventually stabilizing. At the cessation of the final dynamic shear stress wave, the shear zone possesses a small but noticeable velocity. This observation indicates that the shear resistance at that moment is lower than the mean value of the dynamic load, and thus provides the initial velocity for the postseismic creep. As illustrated in Fig. 6*B*, under slow strain rates, the shear resistance may gradually recover due to healing effects. Once the shear resistance surpasses the applied shear stress, the shear deformation decelerates and ultimately ceases.

The healing effect, also referred to as slow dynamics, force relaxation, or aging, reflects the time-dependent behavior of friction within granular materials (11, 16, 37). This phenomenon can arise from mechanisms operating at multiple scales. At the microscale, plastic deformation of asperity contacts strengthens the bonds between contacts (16, 37). At the mesoscale, particle rearrangements, particularly within confined environments, contribute to the healing process of the granular material (38).

The healing effect exhibits a strong rate dependency. It is most pronounced when the granular system is at rest. Conversely, continuous shear strain can disrupt the healed contacts, leading to strength degradation. However, healing can still occur, albeit less effectively, under slow sliding motion. In such conditions, a dynamic equilibrium state emerges between the breaking and regeneration of asperity contacts (37). This mechanism provides a possible explanation for the rate-dependent behavior observed in granular materials (39). Postseismic healing is defined as follows:

Postseismic healing: The increase in shear strength of a granular shear zone as time lapses after vibration. The healing effect is most significant in static conditions and decreases with increasing sliding velocity, thus becoming negligible during rapid motion.

The healing effect follows a logarithmic law, increasing the friction coefficient with time (11, 38):

$$\mu(t) = \mu_1 + B \cdot \ln\left(\frac{t}{t_0} + 1\right), \quad [2]$$

where μ_1 is the shear resistance coefficient when dynamic loading stops and thus the healing effect becomes evident. t is the healing duration, t_0 is a characteristic time scale, and B is a parameter representing the healing rate. The value of B and t_0 can be also influenced by the confining stress state and the shear strain rate (11, 37).

Once dynamic loading stops, the healing effect leads to a gradual increase in shear resistance if the shear zone is static or slow-creeping. If the coseismic weakening had reduced the shear resistance to a value significantly below the applied shear stress, the shear zone would undergo rapid slip, causing the healing effect negligible and ultimately leading to shear zone failure (as in Fig. 6*C*). However, as depicted in Fig. 6*B*, if the shear resistance after dynamic weakening remains only slightly below the applied shear stress, the postseismic sliding will be extremely slow. In this scenario, the healing effect can progressively compensate for the seismic-induced weakening. This balance of weakening and healing results in a transition from accelerating to decelerating postseismic creep, ultimately leading to shear zone stable.

Metastable State. The aforementioned mechanisms provide a framework for understanding the three distinct scenarios observed in our experiments. Fig. 8 schematically illustrates the relationship between the coseismic weakening curve, applied shear stress, and dynamic cycles, allowing for a preliminary prediction of shear zone behavior under dynamic loading. This interplay between coseismic weakening and postseismic healing influences the granular shear zone's response. Fig. 8 presents the results of experiments conducted under a constant normal stress of 300 kPa with a dynamic shear stress amplitude of 25 kPa at a frequency of 1 Hz, while the applied shear stress varies from 182 to 196 kPa. We observe that higher applied shear stress levels lead to instability with fewer cycles.

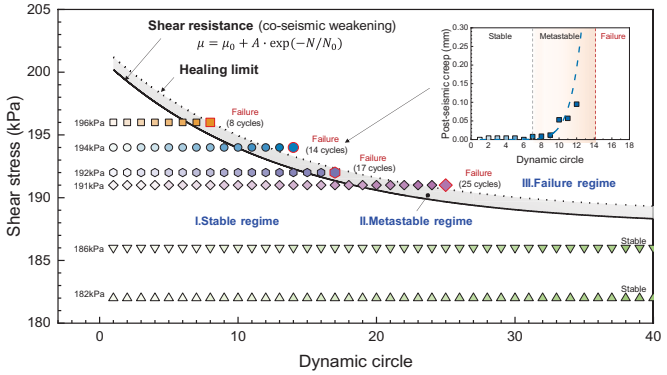

Fig. 8. Schematic diagram of the stable regime, metastable regime, and failure regime. Data are from experiments with varying applied shear stress. The relationship between applied shear stress, shear resistance, and dynamic cycles determines the dynamic response of granular shear zone.

Conversely, at sufficiently low applied shear stress, the shear zone can remain stable even after 40 dynamic cycles.

These observations allow us to classify the dynamic response into three distinct regimes:

1) Stable Regime: In this regime, shear resistance does not weaken below the applied shear stress. Coseismic slip is induced by the peak value of the dynamic load. During the postseismic phase, shear resistance is higher than the applied shear stress, resulting in almost no postseismic creep.
2) Metastable Regime: As dynamic cycles increase, shear resistance progressively weakens, eventually approaching or falling below the applied shear stress. This leads to continued deformation during the postseismic phase (Fig. 6*B*). The postseismic creep will become more significant with increasing dynamic cycles. The healing effect is still obvious due to the relatively lower shear strain rate. When the shear resistance recovers and even surpasses the applied shear stress, the shear deformation decelerates and eventually stops. This regime is not fully stable; a slight disturbance, such as a fast stick–slip event, may trigger the instability of the shear zone due to the rate-dependent effect of the granular flows, hence the term "metastable." This regime may correspond to the postseismic slow-moving landslides.
3) Failure Regime: When subjected to a sufficiently high number of dynamic cycles, the shear resistance weakens substantially, falling significantly below the applied shear stress. The resulting high shear strain rate suppresses the healing effect, rendering the failure irreversible. During the postseismic phase, the persistent imbalance between the weakened shear resistance and the applied shear stress drives continuous acceleration of deformation, ultimately leading to shear zone failure. Under high-intensity seismic conditions, the shear resistance can be drastically reduced compared to the driving force, potentially triggering catastrophic failure directly.

The shear resistance weakening curve depicted in Fig. 8, which serves as the basis for delineating the three regimes, is sensitive to both the frequency and amplitude of the dynamic loading. As demonstrated in *SI Appendix*, Fig. S13, increasing the dynamic amplitude from 25 to 30 kPa, for instance, leads to more pronounced shear resistance weakening and a lower steady-state dynamic friction value. Consequently, in real earthquakes with higher amplitudes, the metastable state or even failure can be easier to be triggered. While the stable and failure regimes can be reasonably anticipated based on our understanding of dynamic weakening in granular materials, the metastable regime highlights the intricate interplay between coseismic weakening and postseismic healing. The metastable state, occurring once the shear zone is near the critical state, is highly sensitive and can easily trigger instability. Our experimental observations imply that the state of a shear zone may be preliminarily estimated based on its response to dynamic loading. As shown in the *Inset* of Fig. 8, when the shear zone is in the metastable regime, an evident increase of postseismic creep can be observed, which is a precursor of shear zone instability.

Modified Prediction Method. The coseismic weakening and postseismic healing effects can be incorporated into the Newmark slide block method (19), a widely used model for predicting dynamic-induced deformation of landslides. The classical Newmark slide block method assumes constant shear resistance. This assumption leads to similar step-like shear displacements in each dynamic cycle when the dynamic load exceeds the shear stress, as shown in Fig. 9*A*. While the classical Newmark method can provide a general explanation for seismic-induced shear displacement, it fails to accurately capture the nuanced phenomena and distinct dynamic responses observed in our experiments and many in situ observations. Thus, we introduce the coseismic weakening and postseismic healing effect into the prediction model, as depicted in Fig. 9*B*. The motion function of the slid block method can be described as follows:

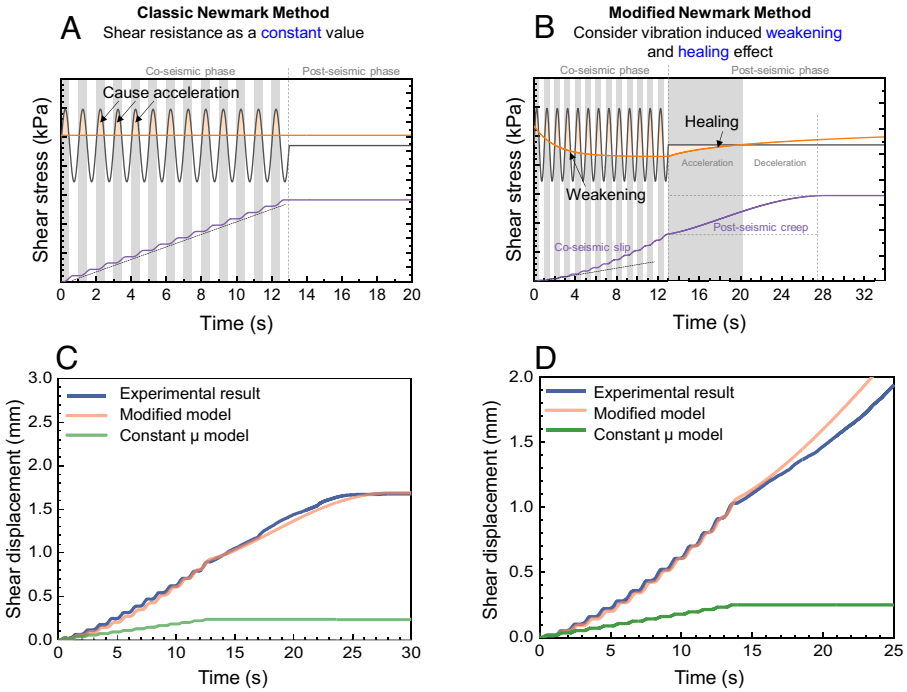

Fig. 9. Comparison of shear deformation prediction between the (*A*) classical and (*B*) modified Newmark methods. The modified Newmark method incorporates both coseismic weakening and postseismic healing, resulting in a more accurate representation of the observed experimental phenomena. (*C* and *D*) Performance comparison of classical and modified Newmark methods in predicting shear deformation. The blue lines represent experimental results, while the orange and green lines represent predictions from the modified and classical Newmark methods, respectively.

$$m\ddot{s}(t) + \mu(N) \cdot F_n \cdot sign[\dot{s}(t)] = F_s(t), \quad [3]$$

where m is the equivalent mass of the sliding block, $s(t)$ is the shear displacement at time t, $\dot{s}(t)$ is the shear velocity, $\ddot{s}(t)$ is the acceleration, and $\mu(N)$ is the friction of the granular shear zone, which gradually decayed with dynamic cycles as described in Eq. **1**, and may increase during the postseismic phase as described in Eq. **2**, F_s is the applied shear force in the experiments, F_n is the stress in the normal direction, and the *sign* function demonstrates that the shear resistance is opposite to the direction of the velocity.

In the experimental case, the dynamic load is sinusoidal, and the friction is gradually weakened during the coseismic phase following Eq. **1**. Therefore, Eq. **3** can be expressed as

$$m\ddot{s}(t) + \left[\mu_0 + A \cdot \exp\left(-\frac{t}{T \cdot N_0}\right)\right] \cdot F_n \cdot sign[\dot{s}(t)] = \overline{F_s} + \Delta F \cdot \sin(2\pi t), \quad [4]$$

where T is the period of the dynamic load, and $\overline{F_s}$ and ΔF represent the mean value and amplitude of the dynamic shear stress, respectively.

During the postseismic phase, the healing effect will gradually strengthen the shear resistance. The shear displacement can be predicted by incorporating a healing Eq. **2**.

$$m\ddot{s}(t) + \left[\mu_1 + B \cdot \ln\left(\frac{t}{t_0} + 1\right)\right] \cdot F_n \cdot sign[\dot{s}(t)] = \overline{F_s} \cdot \quad [5]$$

Eqs. **4** and **5** can be solved numerically using the Euler method to predict shear deformation. Thus, we can predict the shear displacement during both the coseismic and postseismic phases. The results of this modified Newmark model are presented in Fig. 9 *C* and *D*.

The modified Newmark method, accounting for both coseismic weakening and postseismic healing, demonstrates a significant improvement in predictive accuracy compared to the classical approach. The modified model accurately replicates both the nonlinear increase of shear deformation during each dynamic cycle and the observed postseismic creep behavior. Furthermore, unlike the classical Newmark method, which cannot predict shear zone instability and failure, the modified model, incorporating dynamic weakening mechanisms, accurately predicts both coseismic deformation and the shear zone failure observed in our experiments.

Implications. The experimental phenomena observed in this study may shed light on the mechanisms underlying various interesting landslide behaviors, such as earthquake-accelerated landslides, delayed-trigger landslides, as well as the triggering mechanisms of catastrophic coseismic landslide failure (6–10).

The three types of dynamic response of the shear zone observed in our experiments (Fig. 6 *A*–*C*) may correspond to the mechanisms of different types of real landslide behavior during earthquakes.

- In regions experiencing weak seismic intensity, slopes may deform during an earthquake but quickly stabilize after the shaking ceases. This corresponds to the stable state shown in Figs. 6*A* and 8, characterized by coseismic slip but no postseismic deformation.
- In regions with moderate seismic intensity, landslides may exhibit long-term slow creeping after an earthquake, eventually stabilizing after days or months. This behavior, termed earthquake-accelerated landslides (7–10), has been reported in earthquake-prone regions such as southern Peru (7–9), central Italy (10), Georgia (6), and China (3, 40, 41). These landslides display postseismic deformation including acceleration, stabilization, and deceleration phases (10). This scenario is analogous to the metastable state observed in our experiments (Figs. 6*B* and 8), characterized by pronounced postseismic creep that eventually ceases spontaneously. Previous studies have attributed postseismic slip to rate-and-state friction (7, 10, 42, 43). However, our experimental work suggests that, in addition to rate-dependent behavior, seismic-induced weakening and the subsequent healing effect within the shear zone may play a crucial role in influencing earthquake-accelerated landslides.
- In regions experiencing high seismic intensity and on steep slopes, landslides may fail catastrophically. This corresponds to the failure state shown in Figs. 6*C* and 8. If the shear resistance of the shear zone is weakened just beyond the healing limit and into the failure regime (Fig. 8), the slope may undergo slow but irreversible failure. This scenario may explain some delayed-triggered landslides observed after earthquakes, such as the Wangjiayan landslide, which caused 1,600 fatalities near the epicenter of the Wenchuan earthquake. Eyewitness reports indicate that this landslide failed 10 min after the main shock (44). Furthermore, if the seismic intensity is extremely high, drastically weakening the shear resistance compared to the driving force, the landslide will experience catastrophic failure. In this condition, the shear zone will directly surpass its metastable state and transfer into catastrophic failure.

It is important to note that the seismic intensity mentioned above is not an absolute value but is relative to the stress state of the slope and the mechanical properties of the shear zone.

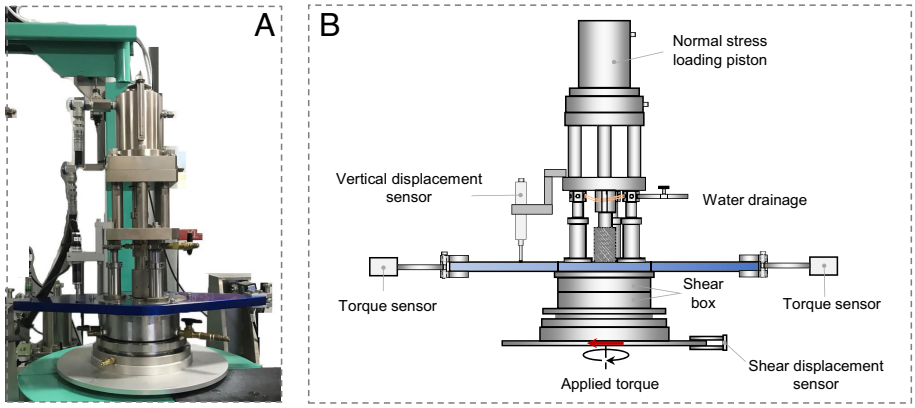

Fig. 10. ICL2 dynamic ring shear apparatus. (*A*) The photo and (*B*) the schematic diagram.

The coseismic weakening and postseismic healing effects are observed not only in our mechanical simulations but also can be inferred from in situ monitoring data (9, 10). The in situ postseismic creep resembles the analog deformation patterns observed in the experiments. This correspondence between our experimental findings and field observations demonstrates that the mechanisms identified in this work will enhance our understanding of the inherent physics in real earthquake-induced landslides. However, recognizing that real landslides involve geological processes and material complexity, a gap remains between our idealized experimental work and the intricacies of natural systems. Bridging this gap will require extensive future research.

Materials and Methods

An ICL-2 dynamic ring shear apparatus (Fig. 10) was employed to simulate the dynamic shear behavior of granular shear zones. This apparatus allows for the application of dynamic loads to both normal and shear stress components. The experimental setup comprises an annular shear box with inner and outer diameters of 10 cm and 14.2 cm, respectively, and a height of 5.2 cm. A rotating bottom plate applies torque to the sample, and shear stress is continuously measured using a pair of torque sensors mounted on the top plate. Synchronous recordings of shear displacement, normal stress, and sample height are acquired throughout the experiments.

Following the previous methods (11, 14, 16, 23), glass beads with a diameter of 0.2 to 0.4 mm were chosen as an ideal granular material. This choice minimizes particle crushing (within the stress state of this work), shape effects, and the possible crystallization of monodisperse spheres, allowing for a more fundamental understanding of granular shear zone dynamics. A consistent initial packing density (1.53 g/cm^3) was achieved by carefully layering a predetermined weight of glass beads and designed sample height into the shear box.

Prior to dynamic loading, each sample underwent consolidation under 300 kPa normal stress, followed by preshearing at a constant velocity of 0.5 mm/s to a steady state (characterized by stable shear resistance and sample height). Upon achieving a steady state, the experiment transitioned from a strain-controlled to a stress-controlled mode (Fig. 1*D*). Due to the lower strain rates associated with stress-controlled conditions and the inherent rate-dependent behavior of the material, slightly higher shear stress could be applied without inducing shear zone failure. Earthquakes are more likely to trigger landslides that are already nearing their critical state. To investigate the response of the shear zone to dynamic loading, we applied varying levels of shear stress within a range near the steady-state friction but remaining below the failure threshold. Applying shear stress significantly below this range does not induce observable postseismic behavior. Conversely, exceeding this range may trigger static failure even without (or with minimal) dynamic loading. Each sample was then subjected to an increasing number of simple harmonic waves, starting with one cycle and continuing until either failure occurred or the material stabilized after more than about 40 cycles. A comprehensive list of experimental parameters is provided in *SI Appendix*, Table S1. Experiments were conducted under dynamic shear stress (experiments S01–S10) or dynamic normal stress (experiments N01–N06) loading conditions, and the detailed experimental data are provided in *SI Appendix*, Figs. S14–S29.

Data, Materials, and Software Availability. Datasets have been deposited in Figshare (https://doi.org/10.6084/m9.figshare.27024340.v5) (45). All other data are included in the article and/or *SI Appendix*.

ACKNOWLEDGMENTS. We are supported by the National Natural Science Foundation of China (NSFC) for Distinguished Young Scholars of China (42325703), the National Basic Research Program of China: basic research funding (42090051), the NSFC funding (42477207), and Sichuan Science and Technology Program (2021JDTD0014).

Author affiliations: [a]State Key Laboratory of Geo-Hazard Prevention and Geo-Environment Protection, Chengdu University of Technology, Chengdu 610059, China; [b]Department of Civil and Environmental Engineering, University of Massachusetts, Amherst, MA 01003; and [c]Institut Langevin, École Supérieure de Physique et de Chimie Industrielles de la Ville de Paris, Université Paris Sciences & Lettres, CNRS, Paris 7587, France

1. P. Meunier, N. Hovius, A. J. Haines, Regional patterns of earthquake-triggered landslides and their relation to ground motion. *Geophys. Res. Lett.* **34**, L20408 (2007).
2. P. Meunier, N. Hovius, A. J. Haines, Topographic site effects and the location of earthquake induced landslides. *Earth Planet. Sci. Lett.* **275**, 221–232 (2008).
3. R. Q. Huang, X. M. Fan, The landslide story. *Nat. Geosci.* **6**, 325–326 (2013).
4. T. Togo, T. Shimamoto, J. J. Dong, C. T. Lee, C. M. Yang, Triggering and runaway processes of catastrophic Tsaoling landslide induced by the 1999 Taiwan Chi-Chi Earthquake, as revealed by high-velocity friction experiments. *Geophys. Res. Lett.* **41**, 1907–1915 (2014).
5. W. Hu *et al.*, Effect of amplitude and duration of cyclic loading on frictional sliding instability in granular media: Implication to earthquake triggering of landslides. *J. Geophys. Res. Solid Earth* **127**, e2022JB024488 (2022).
6. R. W. Jibson, C. S. Prentice, B. A. Borissoff, E. A. Rogozhin, C. J. Langer, Some observations of landslides triggered by the 29 April 1991 Racha earthquake, Republic of Georgia. *Bull. Seismol. Soc. Am.* **84**, 963–973 (1994).
7. P. Lacroix, H. Perfettini, E. Taipe, B. Guillier, Coseismic and postseismic motion of a landslide: Observations, modeling, and analogy with tectonic faults. *Geophys. Res. Lett.* **41**, 6676–6680 (2014).
8. P. Lacroix, E. Berthier, E. T. Maquerhua, Earthquake-driven acceleration of slow-moving landslides in the Colca Valley, Peru, detected from Pléiades images. *Remote Sens. Environ.* **165**, 148–158 (2015).
9. N. Bontemps, P. Lacroix, E. Larose, J. Jara, E. Taipe, Rain and small earthquakes maintain a slow-moving landslide in a persistent critical state. *Nat. Commun.* **11**, 780 (2020).
10. C. Song *et al.*, Triggering and recovery of earthquake accelerated landslides in Central Italy revealed by satellite radar observations. *Nat. Commun.* **13**, 7278 (2022).
11. P. A. Johnson, X. Jia, Nonlinear dynamics, granular media and dynamic earthquake triggering. *Nature* **437**, 871–874 (2005).
12. J. Gomberg, P. Johnson, Dynamic triggering of earthquakes. *Nature* **437**, 830–830 (2005).
13. E. E. Brodsky, N. J. van der Elst, The uses of dynamic earthquake triggering. *Annu. Rev. Earth. Planet. Sci.* **24**, 317–339 (2014).
14. B. Ferdowsi *et al.*, Acoustically induced slip in sheared granular layers: Application to dynamic earthquake triggering. *Geophys. Res. Lett.* **42**, 9750–9757 (2015).
15. A. H. Clark, H. J. Nasrin, S. E. Taylor, E. E. Brodsky, Frictional weakening of vibrated granular flows. *Phys. Rev. Lett.* **130**, 118201 (2023).
16. X. Jia, T. Brunet, J. Laurent, Elastic weakening of a dense granular pack by acoustic fluidization: Slipping, compaction, and aging. *Phys. Rev. E* **84**, 020301 (2011).
17. J. Léopoldès, G. Conrad, X. Jia, Onset of sliding in amorphous films triggered by high-frequency oscillatory shear. *Phys. Rev. Lett.* **110**, 248301 (2013).
18. Y. Yuan *et al.*, From creep to flow: Granular materials under cyclic shear. *Nat. Commun.* **15**, 3866 (2024).
19. N. M. Newmark, Effects of earthquakes on dams and embankments. *Géotechnique* **15**, 139–160 (1965).
20. G. H. Wang, R. Q. Huang, S. D. N. Lourenço, T. Kamai, A large landslide triggered by the 2008 Wenchuan (M 8.0) earthquake in Donghekou area: Phenomena and mechanisms. *Eng. Geol.* **182**, 148–157 (2014).
21. K. Sassa, H. Fukuoka, G. H. Wang, N. Ishikawa, Undrained dynamic-loading ring-shear apparatus and its application to landslide dynamics. *Landslides* **1**, 7–19 (2004).
22. S. H. Cui, G. H. Wang, X. J. Pei, R. Q. Huang, T. Kamai, On the initiation and movement mechanisms of a catastrophic landslide triggered by the 2008 Wenchuan (Ms 8.0) earthquake in the epicenter area. *Landslides* **14**, 805–819 (2016).
23. P. A. Johnson, H. Savage, M. Knuth, J. Gomberg, C. Marone, Effects of acoustic waves on stick-slip in granular media and implications for earthquakes. *Nature* **451**, 57–60 (2008).
24. Z. Liao, J. C. Chang, Z. Reches, Fault strength evolution during high velocity friction experiments with slip-pulse and constant-velocity loading. *Earth Planet. Sci. Lett.* **406**, 93–101 (2014).
25. K. Taslagyan, *The Shear Strength of Granular Soils under the Influence of Vibration* (University of Alberta, 2014).
26. L. H. Tong, B. Qi, C. Xu, Fluidity characteristic of granular materials within low frequency dynamics. *Int. J. Mech. Sci.* **202**, 106508 (2021).
27. W. Ye *et al.*, Experimental study on dynamic characteristics of granular materials under axial high-frequency vibration. *Acta Geotech.* **17**, 3211–3227 (2022).
28. H. Sone, T. Shimamoto, Frictional resistance of faults during accelerating and decelerating earthquake slip. *Nat. Geosci.* **2**, 705–708 (2009).
29. S. Aretusini, F. Meneghini, E. Spagnuolo, C. W. Harbord, G. Di Toro, Fluid pressurisation and earthquake propagation in the Hikurangi subduction zone. *Nat. Commun.* **12**, 2481 (2021).
30. C. Harbord, N. Brantut, E. Spagnuolo, G. Di Toro, Fault friction during simulated seismic slip pulses. *J. Geophys. Res. Solid Earth.* **126**, e2021JB022149 (2021).
31. J. Chen, L. B. Hunfeld, A. R. Niemeijer, C. J. Spiers, Fault weakening during short seismic slip pulse experiments: The role of pressurized water and implications for induced earthquakes in the Groningen gas field. *J. Geophys. Res. Solid Earth.* **128**, e2022JB025729 (2023).
32. P. A. Johnson *et al.*, Dynamically triggered slip leading to sustained fault gouge weakening under laboratory shear conditions. *Geophys. Res. Lett.* **43**, 1559–1565 (2016).
33. C. K. C. Lieou, A. E. Elbanna, J. M. Carlson, Dynamic friction in sheared fault gouge: Implications of acoustic vibration on triggering and slow slip. *J. Geophys. Res. Solid Earth.* **121**, 1483–1496 (2016).
34. J. A. Dijksman, G. H. Wortel, L. T. H. van Dellen, O. Dauchot, M. van Hecke, Jamming, yielding, and rheology of weakly vibrated granular media. *Phys. Rev. Lett.* **107**, 108303 (2011).
35. K. Xia, S. Huang, C. Marone, Laboratory observation of acoustic fluidization in granular fault gouge and implications for dynamic weakening of earthquake faults. *Geochem. Geophys. Geosyst.* **14**, 1012–1022 (2013).
36. J. Léopoldès, X. Jia, A. Tourin, A. Mangeney, Triggering granular avalanches with ultrasound. *Phys. Rev. E.* **102**, 042901 (2020).

37. T. Baumberger, C. Caroli, Solid friction from stick–slip down to pinning and aging. *Adv. Phys.* **55**, 279–348 (2006).
38. R. R. Hartley, R. P. Behringer, Logarithmic rate dependence of force networks in sheared granular materials. *Nature* **421**, 928–931 (2003).
39. O. Kuwano, R. Ando, T. Hatano, Crossover from negative to positive shear rate dependence in granular friction. *Geophys. Res. Lett.* **40**, 1295–1299 (2013).
40. X. Fan *et al.*, Spatio-temporal evolution of mass wasting after the 2008 Mw 7.9 Wenchuan earthquake revealed by a detailed multi-temporal inventory. *Landslides* **15**, 2325–2341 (2018).
41. M. Chen *et al.*, The long-term evolution of landslide activity near the epicentral area of the 2008 Wenchuan earthquake in China. *Geomorphology* **367**, 107317 (2020).
42. J. H. Dieterich, "Constitutive properties of faults with simulated gouge" in *Mechanical Behavior of Crustal Rocks,* N. L. Carter, M. Friedman, J. M. Logan, D. W. Stearns, Eds. (American Geophysical Union, Washington, DC, 1981), vol. 24, pp. 103–120.
43. H. Perfettini, J. P. Avouac, The seismic cycle in the area of the 2011 Mw9.0 Tohoku-Oki earthquake. *J. Geophys. Res. Solid Earth.* **119**, 4469–4515 (2014).
44. Q. Xu, Y. R. Li, S. Zhang, X. J. Dong, Classification of large-scale landslides induced by the 2008 Wenchuan earthquake, China. *Environ. Earth Sci.* **75**, 22 (2016).
45. Y. Li, W. Hu, Data from "Metastable state preceding shear zone instability: Implications for earthquake-accelerated landslides and dynamic triggering." Figshare. https://doi.org/10.6084/m9.figshare.27024340.v5. Deposited 12 December 2024.